

Estimation of rotor effective wind speeds using autoregressive models on Lidar data

Giyanani, Ashim; Bierbooms, Wim; van Bussel, Gerard

DOI

[10.1088/1742-6596/753/7/072018](https://doi.org/10.1088/1742-6596/753/7/072018)

Publication date

2016

Document Version

Final published version

Published in

Journal of Physics: Conference Series

Citation (APA)

Giyanani, A., Bierbooms, W., & van Bussel, G. (2016). Estimation of rotor effective wind speeds using autoregressive models on Lidar data. *Journal of Physics: Conference Series*, 753. <https://doi.org/10.1088/1742-6596/753/7/072018>

Important note

To cite this publication, please use the final published version (if applicable). Please check the document version above.

Copyright

Other than for strictly personal use, it is not permitted to download, forward or distribute the text or part of it, without the consent of the author(s) and/or copyright holder(s), unless the work is under an open content license such as Creative Commons.

Takedown policy

Please contact us and provide details if you believe this document breaches copyrights. We will remove access to the work immediately and investigate your claim.

Estimation of rotor effective wind speeds using autoregressive models on Lidar data

This content has been downloaded from IOPscience. Please scroll down to see the full text.

2016 J. Phys.: Conf. Ser. 753 072018

(<http://iopscience.iop.org/1742-6596/753/7/072018>)

View [the table of contents for this issue](#), or go to the [journal homepage](#) for more

Download details:

IP Address: 131.180.130.242

This content was downloaded on 03/02/2017 at 13:46

Please note that [terms and conditions apply](#).

You may also be interested in:

[Autoregressive modelling for rolling element bearing fault diagnosis](#)

H Al-Bugharbee and I Trendafilova

[Causal relations in molecular dynamics from the multi-variate autoregressive model](#)

A. Gorecki, J. Trylska and B. Lesyng

[Mathematical Models for the Calculation of Power Absorbed by Absolute Radiometers](#)

J A Cogno and M A Ezpeleta

[Nanoparticle size measurement from dynamic light scattering data based on an autoregressive model](#)

Z M Li, J Shen, X M Sun et al.

[Random-Lag Singular Cross-Spectrum Analysis](#)

F. Varadi, R. K. Ulrich, L. Bertello et al.

[Normal/independent noise in VIRGO data](#)

F Acernese, P Amico, M Alshourbagy et al.

[Autoregressive model order selection](#)

Dennis J McFarland and Jonathan R Wolpaw

[Randomly fluctuating potential-controlled multistable resonant tunneling current through a quantum dot](#)

Pei Wang, Gao Xianlong and Shaojun Xu

Estimation of rotor effective wind speeds using autoregressive models on Lidar data

A Giyanani, W A A M Bierbooms, and G J W van Bussel

Delft University of Technology, Wind Energy Research Group, Faculty of Aerospace Engineering

Kluyverweg 1, 2629HS Delft, The Netherlands

E-mail: a.h.giyanani@tudelft.nl

Abstract. Lidars have become increasingly useful for providing accurate wind speed measurements in front of the wind turbine. The wind field measured at distant meteorological masts changes its structure or was too distorted before it reaches the turbine. Thus, one cannot simply apply Taylor's frozen turbulence for representing this distant flow field at the rotor. Wind turbine controllers can optimize the energy output and reduce the loads significantly, if the wind speed estimates were known in advance with high accuracy and low uncertainty. The current method to derive wind speed estimations from aerodynamic torque, pitch angle and tip speed ratio after the wind field flows past the turbine and have their limitations, e.g. in predicting gusts. Therefore, an estimation model coupled with the measuring capability of nacelle based Lidars was necessary for detecting extreme events and for estimating accurate wind speeds at the rotor disc. Nacelle-mounted Lidars measure the oncoming wind field from upto 400m(5D) in front of the turbine and appropriate models could be used for deriving the rotor effective wind speed from these measurements. This article proposes an auto-regressive model combined with a method to include the blockage factor in order to estimate the wind speeds accurately using Lidar measurements. An Armax model was used to determine the transfer function that models the physical evolution of wind towards the wind turbine, incorporating the effect of surface roughness, wind shear and wind variability at the site. The model could incorporate local as well as global effects and was able to predict the rotor effective wind speeds with adequate accuracy for wind turbine control actions. A high correlation of 0.86 was achieved as the Armax modelled signal was compared to a reference signal. The model could also be extended to estimate the damage potential during high wind speeds, gusts or abrupt change in wind directions, allowing the controller to act appropriately under extreme conditions.

1. Introduction

Wind turbine controls employ algorithms based on aerodynamic torque, pitch angle and tip speed ratio to estimate the rotor effective wind speeds [1]. These wind speeds are derived based on the wind flow past the rotor and thus, the estimation can only validate the control action already performed by the turbine. In case of extreme events, e.g. gusts, an adequate amount of preview time and preventive control strategy was required, which was not fulfilled by these estimation algorithms. Other methods using Lidars, extrapolate the wind speed measurements from far-field assuming Taylor's frozen turbulence to estimate the wind speeds at the rotor [2], [3], [4]. However, the effects of wind turbine blockage(induction zone), the atmospheric and site conditions were not considered in these estimations [5], [6].



The potential of using Lidars for deriving the rotor effective wind speed has been explored in multiple studies [7], [8], [9], [10]. Taylor's frozen turbulence assumption was generally used for extrapolating the wind speed from the closest measurement range of the Lidar, e.g. 50m, to the rotor, referred to as the rotor effective wind speed. The wind flow field is generally affected by the surface roughness, characterised as roughness length at a particular site. The higher the roughness of the earth's surface, the more the drag on the wind and slower the wind flow. The number of obstacles such as trees, houses and their distances to the turbine also result in substantial decrease in the wind speed flowing towards the wind turbine [11], [12], [13], [14]. Additional variability in the flow field was caused due to the temperature differences, diurnal cycle and changes in the wind direction [13], [15]. While applying Taylor's frozen turbulence for rotor effective wind speed estimation, no consideration was made for the evolution of wind which is affected by the site conditions, the blockage effects of the turbine and ever-changing physical nature of the wind as shown in Fig. (1). This results in a significant mismatch between the estimated rotor effective wind speed and the actual wind speed hitting the rotor [16], [17]. The wind turbine characteristics, the control strategies and the mean wind speed influence the intensity of the blockage effect on the wind flow and act as a source of error in wind speed estimation. Additionally, the total uncertainty increases as more parameters as employed into the rotor-effective wind speed estimation model

This article proposes an auto-regressive model to estimate the rotor effective wind speed with low uncertainty using nacelle-mounted Lidars. The flow of the wind-field from 185m away to 50m in front of the wind turbine can be modelled by using the Autoregressive Moving Average Exogenous, Armax, model to understand its evolution and dissolution. The Armax model is an extension of the ARX model, where a moving average was fitted to the stochastic noise model, while the ARX contributes to the deterministic estimation of the model. The model was trained on past measurements, which allows predicting the future wind speeds at the rotor. The change in the turbulence structure and the evolution of the wind field were modelled as a noise input to the Armax model. In this way, the turbulence structure could be unfrozen and modelled using the measurements at every Lidar range. The uncertainty in the wind speed estimation was derived from the root mean square error for the model achieved by validating the data on future inputs and outputs. The auto-regressive model was then coupled with the blockage factor fitted on Lidar measurements, introduced by Medici [18] for the effects of wind turbine blockage on the upstream wind field. Finally, the wind speed estimations from the combined model were compared for their performance against the estimations from Taylor's frozen turbulence assumption and ECN's model. ECN's model derives the wind speed using lookup tables from aerodynamic torque, blade pitch angle and turbine properties.

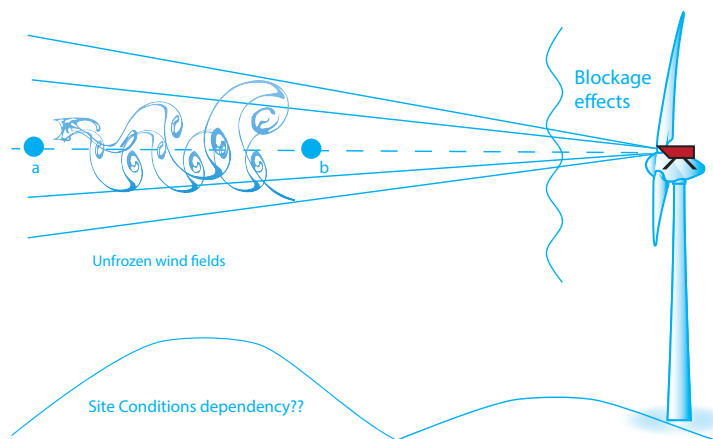


Figure 1: Understanding the physical evolution of wind using Lidars.

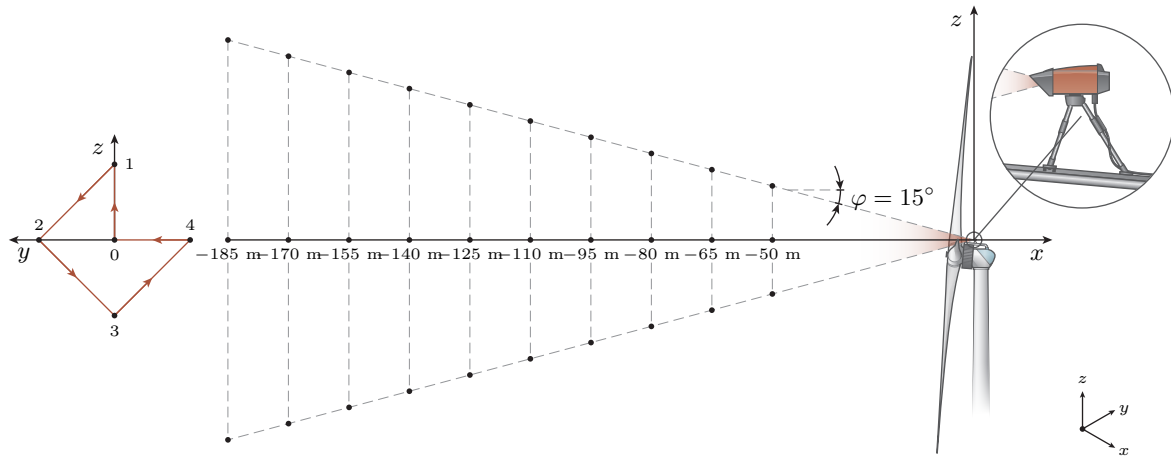


Figure 2: Drawing of the pulsed Lidar system, mounted on the nacelle of a Darwind XD115-5MW wind turbine [21].

2. Method

2.1. Measurement setup

The experimental setup consists of an Avent five beam pulsed Lidar installed on a Darwind XD-115 wind turbine at ECN's wind turbine test site in Wieringermeer as shown in Fig. (2). The hub height of the turbine was 100m above the ground level with a rotor diameter of 115m. The test site is a simple site with flat terrain and distant houses along with some rows of trees. The Lidar has five beams measuring radial wind speeds, RWS_i , upwind of the turbine, where $i = 0, 1, \dots, 4$. The central beam RWS0 was oriented in the longitudinal direction with no cone angle, while the other beams were directed outwards at a cone angle of 15° from the central beam. Each beam was sampled at 4 Hz, ($T_s = 0.25\text{sec}$) according to the scanning pattern shown on the left side of Fig. (2). Thus, a complete cycle was completed in 0.8 Hz ($t_s = 1.25\text{sec}$). The wind speed measurements were performed at range gates from 185m up to 50m in front of the wind turbine with a separation distance of 15m between two ranges. The wind speed time series were filtered for anomalies like spikes, out of range values and low availability. All these data were interpolated using cubic spline for higher Lidar availability. The estimated rotor effective wind speed \bar{U}_{we} , is a function of the measured pitch angle β_p , the aerodynamic torque Γ_r and the rotor speed Ω_r , achieved with the help of lookup tables implemented into ECN's model [19], [20]. \bar{U}_{we} was sampled at 64 Hz and hence, it was downsampled to match the sampling frequency of the Lidar measurements. The \bar{U}_{we} signal is very noisy due to tower fluctuations and other disturbances and therefore a Savitzky golay filter with a smooth factor of 151 along with resampling the signal to 4 Hz was used for deriving correlations.

2.2. Prediction of rotor effective wind speeds using Armax models

The current practise of estimating rotor effective wind speeds assumes Taylor's frozen turbulence hypothesis to be true. This assumption holds true, if the structure of the turbulence doesn't change, maintaining temporal and spatial homogeneity and following the self-preservation of eddies. The wind field then flows with the same mean wind speed and fluctuation, shifting only in time when measured at different Lidar ranges. A minimum preview time of 2 seconds was required by the wind turbine controllers to execute a control action as observed by some studies [2], [22], [23]. Therefore, the nearest Lidar measurement to the wind turbine was deemed to be applicable for online prediction in this study. A wind speed time series at $\Delta x = 50\text{m}$ in front of the wind turbine was shifted with a time delay of $\tau_T = \Delta x / \bar{U}_{50}$, which would be a suitable

assumption for Taylor's frozen wind field, where \bar{U}_{50} is the mean wind speed at 50m and τ_T is the time delay for frozen wind fields. This frozen model was used later for comparing to the reference model and Armax models

Since, the Taylor's frozen turbulence method was not consistent and was applicable to large eddies only, another method which captures the fluctuations of smaller eddies and at the same time allows for better engineering models has to be chosen. Such a typical state space process model can be illustrated by Fig. (3). The mean deterministic part of the wind was modelled using the moving average component within the model, while the fluctuating stochastic part was modelled using the Autoregressive Exogeneous component in the Armax model. The input and output are denoted by $u(k)$ and $y(k)$ respectively, while the stochastic noise or disturbances are modelled by $e(k)$. A deterministic process, represented by a first order differential equation with a delay of one unit is given by Eq. (1), where the coefficients of deterministic output and input upto $(k - 1)^{th}$ instant were given by a_1 and b_1 respectively . The prediction of $x(k)$ given the knowledge of x and u upto the $(k - 1)^{th}$ instant is given by Eq. (2). The overall model for $y(k)$ can be constructed by assuming that the deterministic and the stochastic effects were additive as shown in Eq. (3), where the prediction of $y(k)$ is given by $\hat{y}(k|k - 1)$.

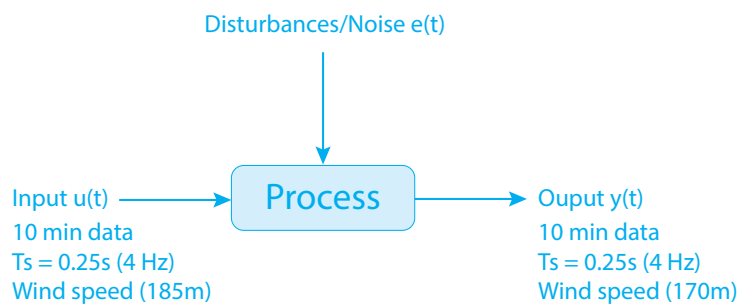


Figure 3: A typical state space process with input, noise and output.

$$x(k) + a_1x(k - 1) = b_1u(k - 1) \quad (1)$$

$$\hat{x}(k|k - 1) = -a_1x(k - 1) + b_1u(k - 1) \quad (2)$$

$$y(k) = u(k) + e(k) \quad (3)$$

$$\hat{y}(k|k - 1) = \hat{u}(k) + \hat{e}(k) \quad (4)$$

The evolution of wind from a Lidar range *point a* to another point *b* was considered to be a linear time invariant (LTI) system, satisfying the principles of homogeneity and superimposition. The time invariance condition states that the system output $y(k)$ does not change as a result of delay in the input $u(k + n_k)$. Thus, the characteristics of the system i.e. wind evolution, are assumed not to change with time. The measured response or output $y(k)$ can be split into two components: deterministic and stochastic. The measured mean wind speed is the deterministic component $x(k)$, while the turbulence, chaos and measurement errors are the stochastic component $e(k)$, where k represents the discrete time period. An Armax model is an extended non-linear, least square auto-regressive estimation model, which incorporates a moving average term in the noise model. It is given by Eq. (5), where B/A and C/A form the deterministic and stochastic coefficients respectively. The expanded form is given by Eq. (6), where n_a , n_b and n_c are the number of parameters in the equation signifying the order of deterministic and stochastic

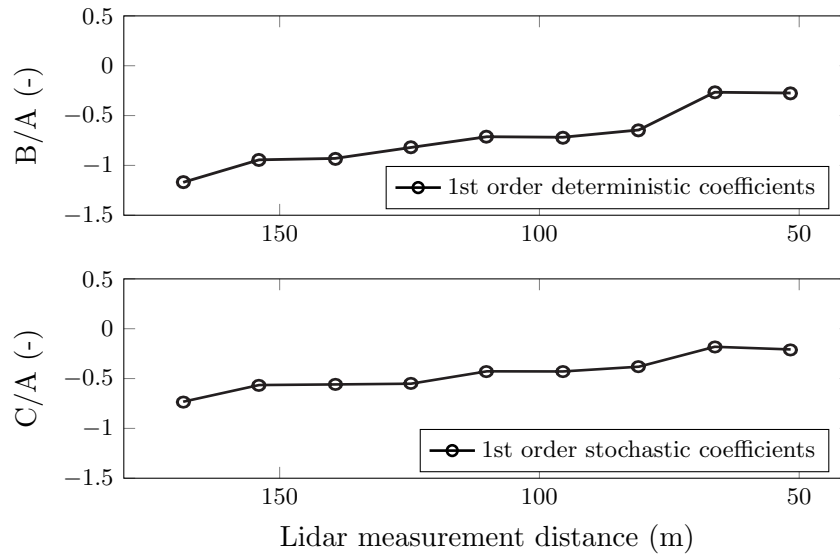


Figure 4: Evolution of deterministic B/A coefficients and stochastic C/A coefficients for first order Armax model over the Lidar measurement distances.

components, while n_k is the delay of the system. (For details, see [24], [25]).

$$\underbrace{Ay(k)}_{\text{Output}} = \underbrace{Bu(k - n_k)}_{\text{Deterministic Input}} + \underbrace{Ce(k)}_{\text{Stochastic Noise}} \quad (5)$$

$$\underbrace{y(k) + a_1 y(k - 1) + \dots + a_{n_a} y(k - n_a)}_{\text{Output}} = \underbrace{b_{n_k} u(k - n_k) + \dots + b_{n_b + n_k - 1} u(k - n_b + n_k - 1)}_{\text{Deterministic Input}} + \underbrace{c_1 e(k - 1) + \dots + c_{n_c} e(k - n_c) + e(k)}_{\text{Stochastic noise Input}} \quad (6)$$

A preliminary analysis using visualization and standard filtering was performed on the time series for input $u(k)$ and output $y(k)$. This step allows to examine the time series for outliers, peaks, trends and data acquisition problems, that were filtered before performing model estimation. The impulse response and the step response were performed to confirm the stability of the model, i.e. it was continuously excited and exhibits linear time invariant behaviour. The impulse response estimates obtained by fitting finite length impulse response model, (FIR), were found to stabilize towards zero, suggesting that the model was stable. The step response reassured a time delay of , $\tau_p = n_k = 1.25s = 5 \text{ samples}$, which represents the time delay between the two measurement sample time series. A closed loop gain of 0.9 and stable step response illustrates that the model was stationary and stable.

As the wind evolves from the Lidar measurement distance of 185m to 170m and subsequently towards the wind turbine as shown in Fig. (2), the state variables B/A and C/A also evolve with different polynomial orders and values. Based on this, the state space model for the current site was determined and predictions of the rotor effective wind speed were performed by step-ahead predictions based on the time delay. The step-ahead predictions of the rotor effective wind speeds, $\hat{y}(k|k - 1)$ were based on past Lidar wind speed measurements $y(k)$ until $(k - 1)$ period, given by Eq. (4). Similarly, $\hat{u}(k|k - 1)$ is the prediction of $u(k)$ given the knowledge of past deterministic and stochastic components. The one-step ahead predictions were performed

mostly to validate the training model, while the infinite-step ahead predictions were performed with validation data in order to determine if the model accounts for global trends as well as local trends. For this purpose, the step-ahead prediction errors are minimized by estimating the A, B and C coefficients accurately. The deterministic and the stochastic coefficients are illustrated in Fig. (4), where the coefficients form a transfer function of the online estimation system. The final expression for predicting one step-ahead and infinite step ahead predictions general equation was given by Eq. (7). Similarly, the state space model for the current experimental configuration for estimating rotor effective wind speeds was given by Eq. (8), where q^{-1} is the backward shift operator representing the time delay in the model. The backward shift operator simply shifts the time by one unit, e.g. $q^{-1}x(k) = x(k - 1)$ and the predictor variable $\hat{y}(k|k - 1)$ means prediction of the output variable $y(k)$ with the knowledge of $(k - 1)$ past observations.

$$\hat{y}(k|k - 1) = \frac{B}{A}u(k) + \frac{C}{A}e(k) \quad (7)$$

$$\hat{y}(k|k - 1) = \frac{0.05q^{-3} - 0.03q^{-4} - 0.01q^{-5} + 0.13q^{-6} - 0.09q^{-7}}{1 - 1.06q^{-1} - 0.5q^{-2} + 0.62q^{-3}}u(k) \dots + \frac{1 - 0.03q^{-1} - 0.53q^{-2}}{1 - 1.06q^{-1} - 0.5q^{-2} + 0.62q^{-3}}e(k) \quad (8)$$

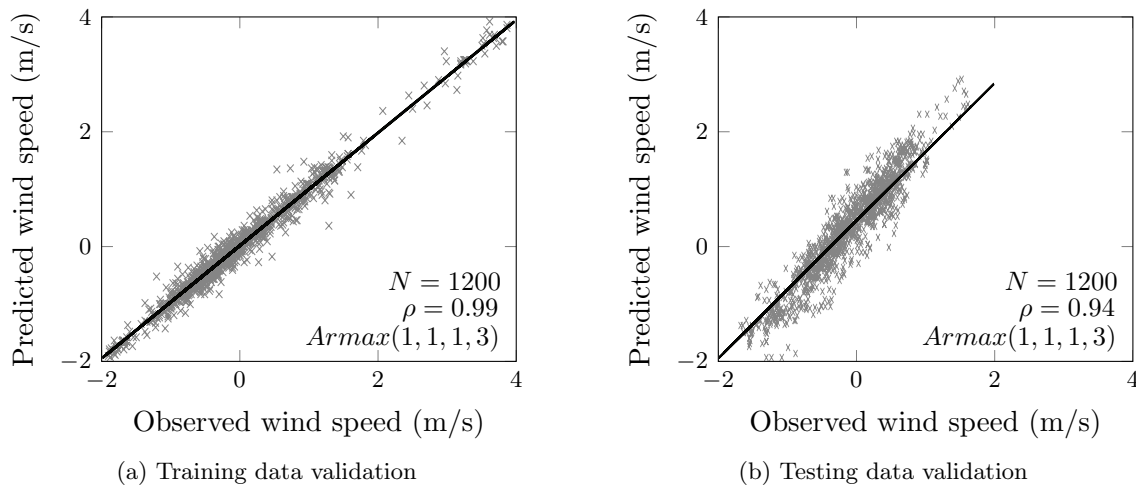


Figure 5: Correlation plots of Armax model predictions with training data and testing data for model quality validation.

The wind speed fluctuation prediction capability using Armax model were evaluated by comparing the Armax model output to measurements at 50m as shown in Fig. (6). The cross-correlation between the predicted wind speed and the observed wind speed for training data, Fig. (5a) was about 0.99, and 0.94 for testing data, Fig. (5b). The high correlation indicates that the model is suitable to perform accurate predictions on fresh datasets. Certain tests like the auto-correlation function and residual error were additionally performed in order to validate the model and reduce the model uncertainty. This model was used further for predicting the wind speeds based on past measured data and future input, e.g. wind speed at 50m as an future input for predicting the wind speed at the rotor plane.

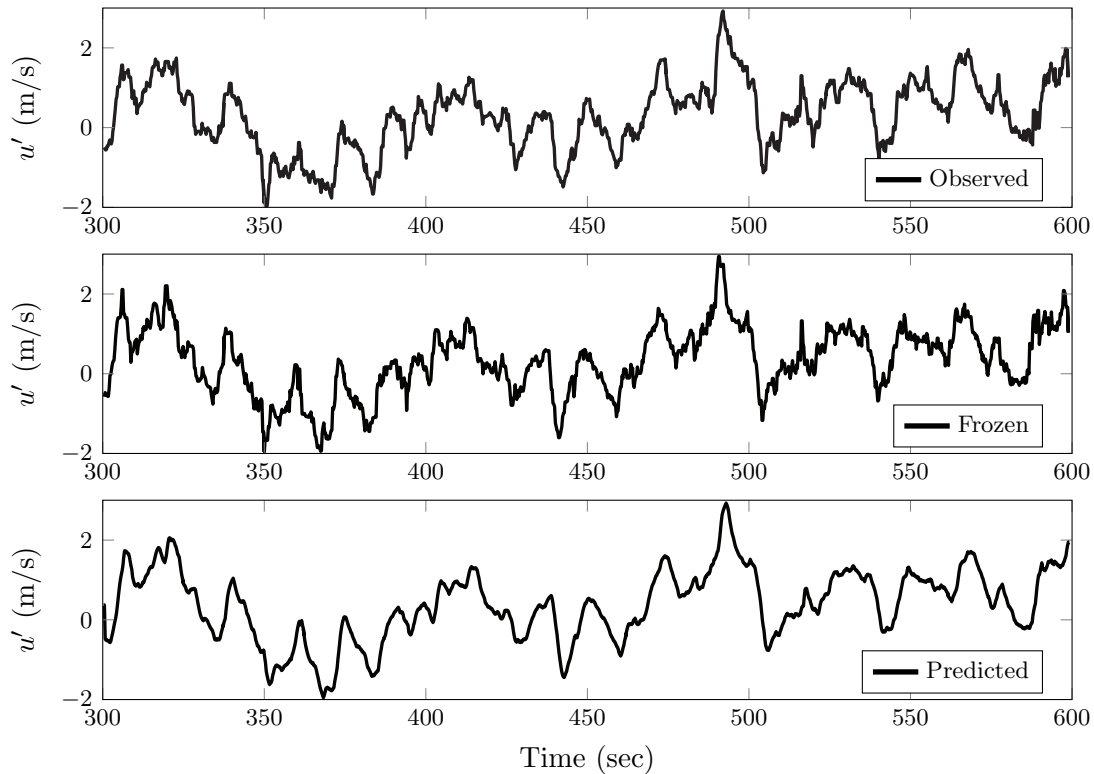


Figure 6: Comparison of the Observed, Frozen, and the Armax predicted wind speed fluctuations.

2.3. Prediction of rotor effective wind speed using blockage factor

The blockage effect from a wind turbine is a phenomenon, where the wind speed decreases gradually from about four diameters upwind of a turbine [5], [22], [17]. Due to blade rotation, the wind flow is accelerated outside of the rotor tip and decelerates at the central rotor plane [26], [16]. This influence from the rotor on the incoming wind field was modelled as a body force in computational fluid dynamic methods like LES, RANS-CFD, etc. The study of this influence of the wind turbine on the incoming field is relatively seldom and provides an opportunity to understand the phenomenon using nacelle based Lidar measurements. Using the Biot-Savart law on Johnson's vortex sheet theory [27], Medici [5] derived an expression, Eq. (9) for velocity upstream to the wind turbine; where U_r is the upstream wind speed at hub height, U_∞ is the undisturbed wind speed, $\varsigma = x/R$ is the non-dimensional distance, where x is the coordinate along the mean wind speed towards the wind turbine and R is the rotor radius. The axial induction factor a is defined as the fractional decrease in the wind speed, calculated from the undisturbed free stream speed and the induced wind speed as shown in Eq. (10). The effects of induction vary with the body forces exerted by the wind turbine on the wind flow, which is related to the thrust force T and can be derived from the actuator disc theory to Eq. (11) [5]. Lidar measurements up to two rotor diameters in front of the wind turbine were used to quantify the blockage factor b and the estimated undisturbed wind speed using the relations Eq. (9), Eq. (11).

$$b = \frac{U_r}{U_\infty} = 1 - a \left[1 + \varsigma(1 + \varsigma^2)^{-1/2} \right] \quad (9)$$

where, a ideally refers to

$$a = \frac{U_\infty - U_r}{U_\infty} \quad (10)$$

$$T = 2\rho\pi R^2 U_\infty^2 a(1 - a) \quad (11)$$

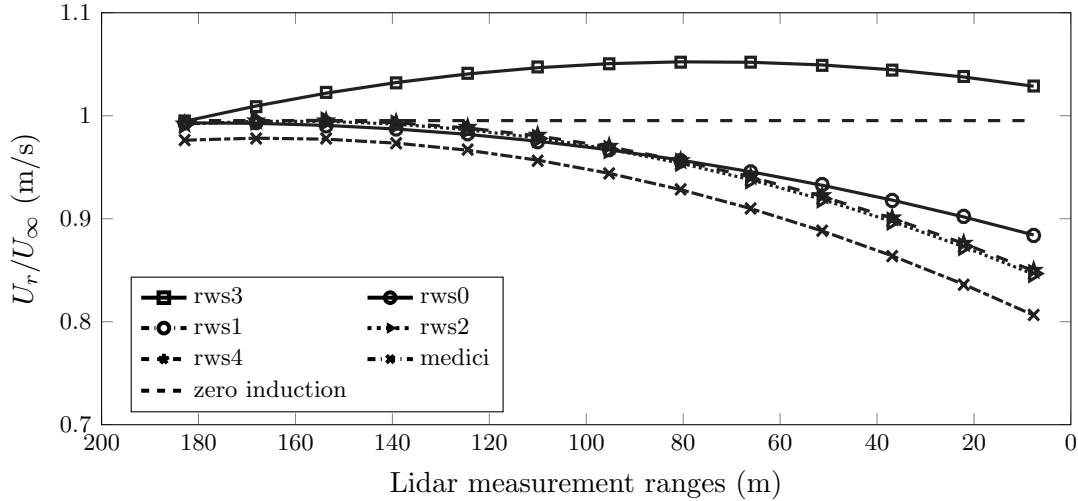


Figure 7: Comparison of the blockage effect from Medici’s theoretical model, Lidar measurements rws 0,1..5, based on 6 months data considering wind speed at 185m as U_∞ .

Medici found through particle image velocimetry PIV, experiments that a wind turbine has a significant effect on the upstream flow and that the effects can extend up to three rotor diameters, whereas the effect was insignificant considering the theoretical Eq. (9). Abdelsalam et al. fitted the Lidar measurements together with Medici’s blockage model to find the axial induction factor. An axial induction factor of $a = 0.27$ fit the fractional decrease in wind speed curve, i.e. U_r/U_∞ well for the experimental conditions given which shall vary according to the control strategy and wind turbine characteristics. It was also observed that a was inversely proportional to the wind speed i.e. at high wind speeds, lower a was observed and vice versa. Simley et al. [17] investigated the error in feed-forward control due to induction zone of Lidar measurements to that of LES models and observed slowing down of wind flow towards the wind turbine. However, Simley could not produce concrete conclusions to justify that the induction zone affected the wind speeds significantly. These results lay the foundation for further studies of blockage effects and wind evolution towards the turbine. When combined with the prediction method using Armax models and Lidar data, it allows us to make accurate predictions for the wind speed at the rotor plane.

The Lidar data measured at consecutive ranges was used for the determination of the blockage factor according to Eq. (9). The data was filtered for anomalies and other atmospheric constraints, e.g. wind speed range between 1 m/s to 35 m/s. Three cases were established in order to study the blockage effect for XD115 turbine at the Lawine test site using the fractional decrease in wind speed, Medici’s equation employed in different ways to use Lidar data appropriately. *Case 1* is the simplest form based on the definition of axial induction factor, Eq. (10), where two range gates, e.g. 110m and 95m were considered. Here, the wind speed at 110m was considered as U_∞ , while the wind speed at 95m as U_r . Each range gate combination provides a mean blockage factor. *Case 2* assumes U_∞ to be the wind speed at 185m for all the combinations, while U_r changes simultaneously towards the turbine. The blockage effect for

all Lidar beams for *Case 2* can be seen in Fig. (7). Every beam except the RWS3 follows the fractional decrease of the wind speed. The effect of the ground accelerating the flow as a walled boundary, similar to the effect in the wind tunnels could be observed. This is confirmed by the LES plots made by Simley et al. [16] and PIV observations by Hong et al. [26]. For *Case 3*, two consecutive Lidar range gates were considered simultaneously, where U_{r1} and U_{r2} are the wind speed time series at each range gate. By solving the simultaneous equations for two range gates, the blockage factor b and the undisturbed wind speed U_∞ could be iteratively approximated. *Case 1* and *Case 2* consist of one unknown parameter b , achieved by solving one equation, while *Case 3* has two unknowns, since it assumes that only the U_r value is known. The Matlab's *solve* function was effectively used to solve multivariate simultaneous equations thus created for the whole time series. The cases are discussed as follows:

Case 1: Simplest form of speed reduction, i.e. $b = U_r/U_\infty$.

Case 2: Assuming wind speed measured at 185m as U_∞ , while U_r is the consecutive Lidar measurement ranges; i.e. $U_\infty = 185m$, $U_r = 185, 170...50m$.

Case 3: Using U_{r1} and U_{r2} from two consecutive Lidar range gates to form two simultaneous equations to solve iteratively for a and U_∞ ; i.e. $U_{r1} = 185m...$, $U_{r2} = 170m...$

The blockage factor for the above cases was determined for ten Lidar ranges from 185m to 50m in front of the wind turbine, each separated with 15m distance apart. In order to determine the rotor effective wind speed, the blockage curves and the U_∞ curves were extrapolated to the rotor. By substituting the extrapolated b and U_∞ into the Cases, the rotor effective wind speed U_r can be calculated. The blockage factor for all three cases and their extrapolated curves for a single 10 minute time series with 4 Hz sampling rate as shown in the Fig. (8) and the results were comparable when other time series are used. For Case 3, the blockage factor at the turbine was given by $b = 0.78$ and the undisturbed wind velocity was $U_\infty = 13.2m/s$. Using these inputs, the actual wind speed at the rotor blade (5m in front of the turbine) can be estimated, which was $U_r = 11.2m/s$. Considering the distance between the estimated wind speed and the last measurement point at 50m, the time delay for the wind fields to reach the turbine can be estimated, therefore $\tau_r = \Delta x f / U_r \approx 16 \text{ lags} \approx 4 \text{ seconds}$, where Δx is the distance between 50m and the wind turbine and f is the sampling frequency. This is the time available for the controller to react after the last measurement was performed, which was less than the preview time restriction of 2 seconds. The U_r and τ_r so achieved, were coupled with the fluctuations achieved with the help of Armax model for comparison with the \bar{U}_{we} from ECN's model.

Table 1: Parameters involved in Medici's equation for the three cases at the rotor plane.

| Cases | U_∞ | b | U_r | τ_r |
|---------------|------------|------|-----------|----------|
| <i>Case 1</i> | 12 m/s | 0.12 | 10.56 m/s | 4.25s |
| <i>Case 2</i> | 13 m/s | 0.38 | 8.8 m/s | 5s |
| <i>Case 3</i> | 13.2 m/s | 0.22 | 11.2 m/s | 4s |

3. Results and Discussions

By predicting the wind speed at regular intervals, a differential equation that evolved towards the wind turbine over a distance of two rotor diameters was derived. The evolution of the Armax model's coefficients from 185m to 50m in front of the turbine using Lidar measurements was studied by using carefully measured experimental data at ECN's test site. Fig. (9) illustrates the mean behaviour of the wind speed which corresponds to the behaviour of deterministic and stochastic coefficients in the Armax equation. Fig. (4) shows the evolution of the deterministic and stochastic coefficients towards the wind turbine. The gradual rise in the deterministic

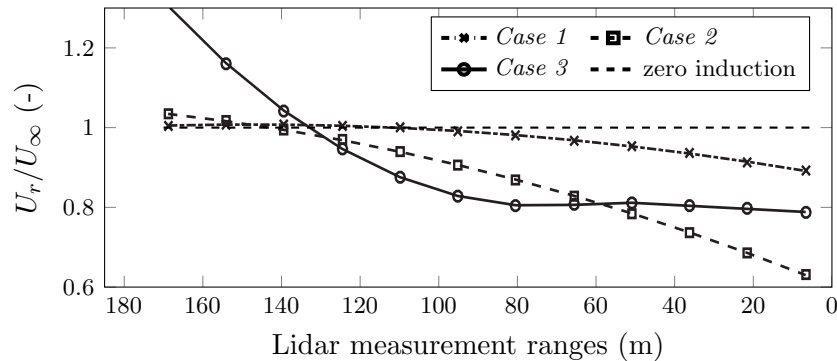


Figure 8: Comparison of blockage factors emerging from three cases defined, extrapolated to the rotor.

and stochastic coefficients suggests non-linearity in the model as the model moves towards the turbine. The Armax prediction model estimates the wind speeds into the future well as can be seen from the Fig. (5b). By combining this prediction of the fluctuation with the different means as shown in Tab. (1), it was possible to derive the rotor effective wind speed as shown in Tab. (2).

Table 2: Comparison of the mean statistics and parameters for wind turbine control.

| Method | U | u' | ρ | τ | Uncertainty |
|-------------------|-------|-------|--------|--------|--------------------|
| Unit | (m/s) | (m/s) | - | sec | % |
| ECN's model | 11.9 | 1.24 | 1.00 | - | 12% |
| Taylor's frozen | 12.3 | 0.73 | 0.87 | 4s | 3.22% |
| Induction + Armax | 11.2 | 0.65 | 0.86 | 4s | 2.56% |
| Armax | 12.3 | 0.65 | 0.86 | 4s | 2% |

Currently, no methods are available to accurately measure or derive the actual rotor effective wind speed. However, the estimated rotor effective wind speeds using ECN's model was used as the most representative signal for comparing different methods. The signal was highly fluctuating with low availability an estimation uncertainty of 12%. The uncertainties in the prediction models are based on the standard error calculation σ/\sqrt{N} and the measurement uncertainty (1%) involved with the Lidar itself. For the Case (Induction+Armax), an additional uncertainty based on the iterative Matlab solver error is introduced. The high uncertainty of the ECN's wind speed signal prohibits to measure the time delay and correlation accurately, which leads to a higher uncertainty in the comparisons itself. The estimated wind speeds represent the thrust force applied on the wind turbine by the energy contained in the wind and thus, the signal was assumed to provide adequate accuracy required for control purposes at present. Considering the high uncertainty involved, the trends and the gust present at approximately 50 seconds and around 490 seconds were accurately modelled by all of the estimation methods and a high correlation, $\rho > 0.85$ was achieved as shown in Tab. (2), even though wind speed estimated by the ECN model does not filter for nodding and tilting of the wind turbine.

The inclusion of the blockage effect along with the predictions of the Armax model present a new direction for using the Lidar measurements with the numerical prediction models for wind turbine control. The blockage effects for the three cases as explained earlier are shown in Fig. (8). The mean wind speed at the rotor is the parameter of interest here and *Case 3* provided the most reasonable estimate for further implementation as can be seen in Tab. (1).

Fig. (9) illustrates the mean statistics of the wind measured for 10 minute time series over a period of 6 months from July 2013 to December 2013, where the effect of blockage

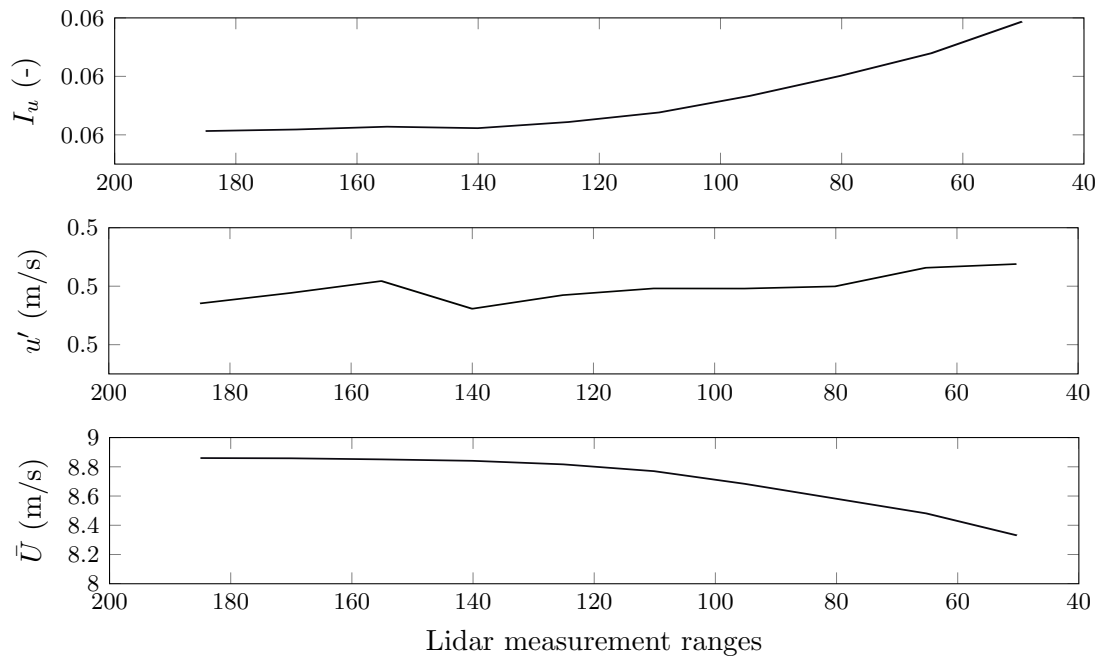


Figure 9: Mean statistics, turbulence intensity(I_u), longitudinal deviation (u') and mean wind speed (\bar{U}) evolution towards the wind turbine.

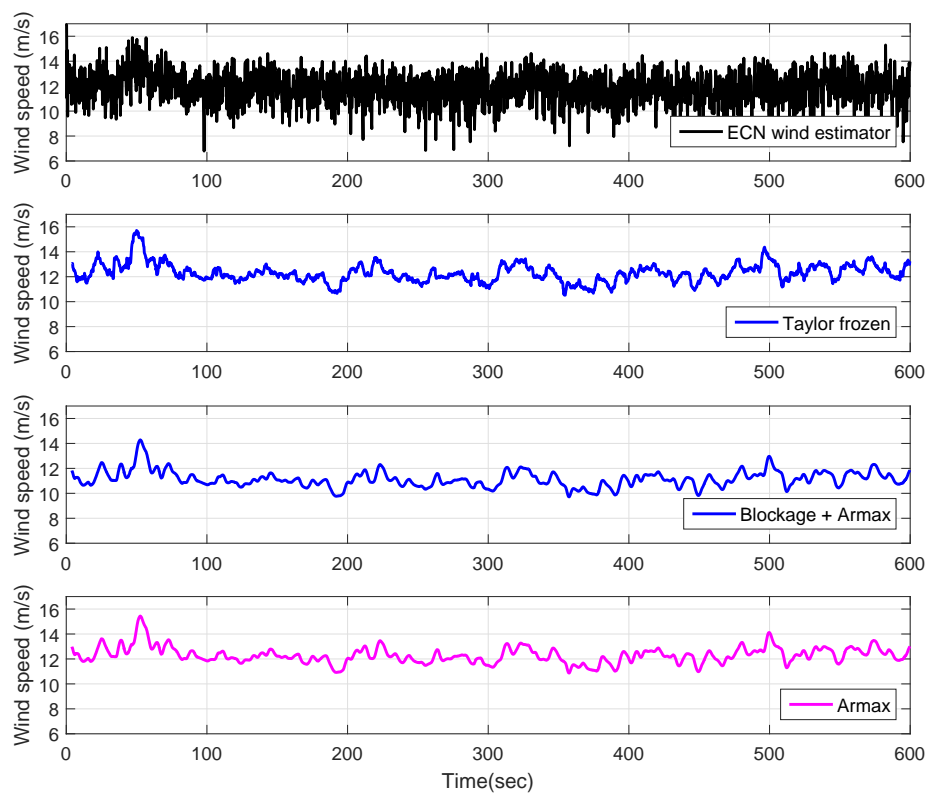


Figure 10: Comparison of wind speed signals from ECN model, frozen model, Induction+Armax model and Armax model.

and higher turbulence intensity could be seen clearly. Tab. (2) shows the time series for all methods compared in this study, where \bar{U}_r is the mean rotor-effective wind speed, u' is the mean deviation, ρ is the correlation coefficient and τ is the time delay between 50m and the rotor. Fig. (10) illustrates the comparison of rotor effective wind speeds estimated using different models discussed i.e. ECN's model, frozen model, the induction plus Armax model and the Armax model. The time delay and the mean wind speeds were adjusted for the corresponding models and for better comparison. The correlation plots for estimated wind speeds using these models were shown in the Fig. (11) and display a high correlation coefficient. Due to the low roughness variation at the test site and due to fluctuating reference wind speed signal, the frozen turbulence assumption performs as good as the Armax modelling. However, there were sufficient studies performed to prove the inapplicability or the restriction of using Taylor's frozen turbulence for wind energy control in all site conditions [17], [28], [29], [30]. The power spectral densities for the different wind speed signals is shown in Fig. (12), where different signals are comparable at low frequencies upto 0.06 Hz. At high frequencies, both the Armax based models were similar, while the frozen turbulence model has higher spectral content suggesting higher variance and thus contributing to a marginally higher correlation with ECN's model. The low variance in the Armax modelling was due to the moving average stochastic model, which filters the signal with a low-pass filter to allow for wind turbine control.

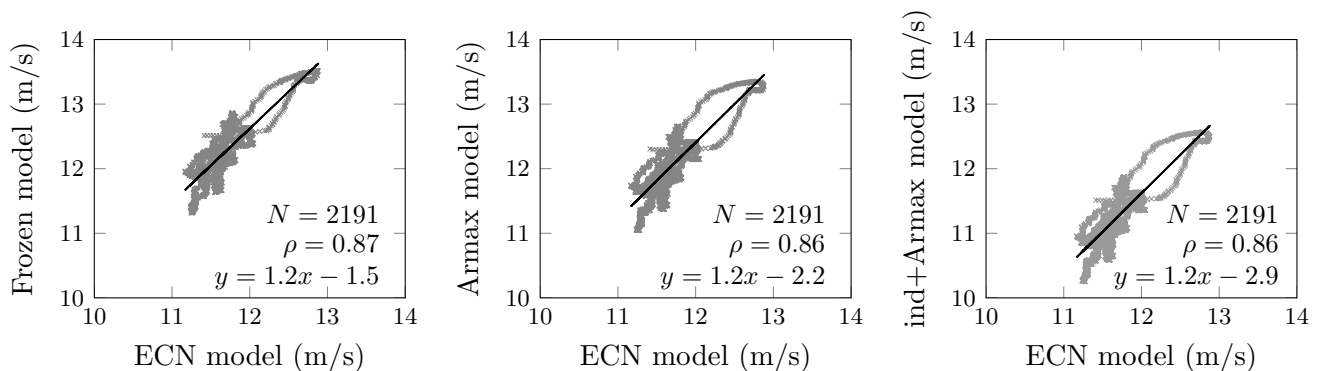


Figure 11: Correlation matrix for wind speed comparisons between the ECN's model and the wind speed predictions (left to right) from Frozen turbulence, Armax and Induction+Armax models.

4. Conclusions

Although the model is yet to be extensively validated, it shows potential for estimating wind speeds with high certainty. Such models incorporating the effects of wind turbine blockage and the prediction capability of the Armax models are seldom found. The Armax model predicted the wind speeds accurately to correlate with the test data with a correlation of $\rho = 0.94$. The evolution of B/A and C/A coefficients towards zero suggest increasingly non-linearity towards the turbine and thus higher disagreement with the linear frozen model. When the individual beams were compared, it was observed that the beams followed the general notion of fractional decrease of wind speed. However, one beam displayed an increase in wind speed marginally, which can be associated with the walled flow concept from wind tunnels. *Case 3* performed the best of all the cases, leading to a mean wind speed of 11.2 m/s, with a blockage factor of $b = 0.78$ and a time delay of $\tau_r = 4sec$, which allows enough time for a wind turbine control action. Initially, a low correlation was observed when the prediction models were compared with the reference ECN's wind speed signal. The highly fluctuating wind speed signal from ECN's model had high frequency terms due to the wind turbine nodding and tilting action and required

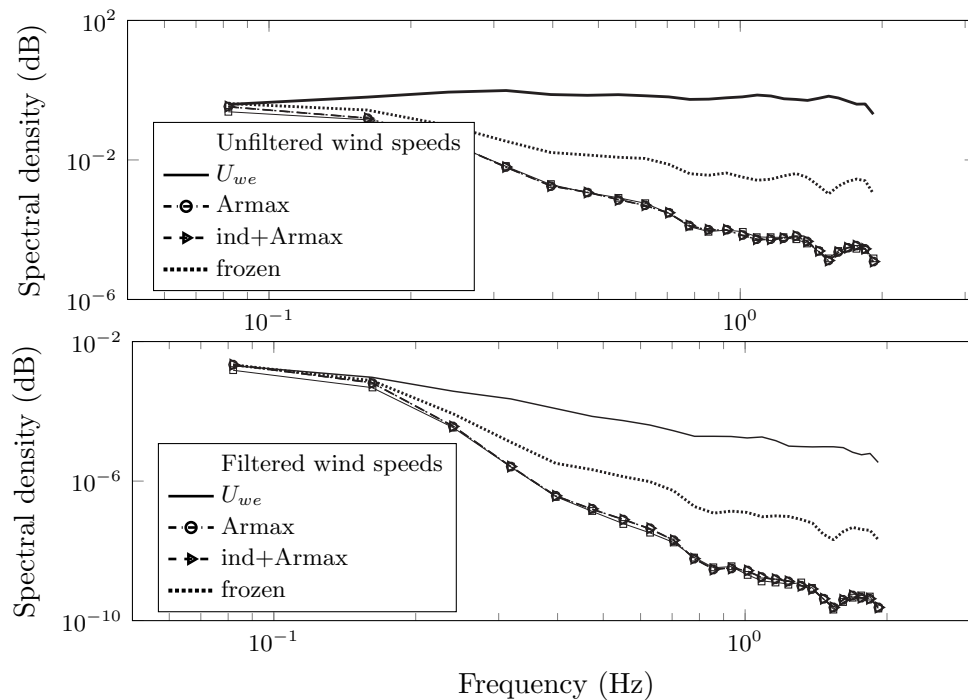


Figure 12: Comparison of power spectral densities for unfiltered (above) and filtered (below) time series of predicted wind speeds using ECN’s model (U_{we}), Armax, Induction+Armax and Taylor’s frozen turbulence model.

low pass filtering for comparison. Before filtering, the correlations were about $\rho = 0.75$ and the correlations improved to about $\rho = 0.86$ after filtering. It was observed with the help of long term measurements that the blockage effect significantly affected the mean wind speed close to the turbine and thus, Taylor’s frozen turbulence has higher uncertainty depending on weather conditions. The different models however display high coherence until 0.06 Hz.

5. Further Work

The model needs to be extensively validated for different conditions, e.g. complex site, blockage effect when the turbines are idle. The model needs to be checked if it can distinguish the effects of wind turbine blockage on the fluctuating part. The sensitivity of the model to surface roughness, wind shear and site and weather conditions shall be pursued. The model can be represented as a transfer function using Eq. (8) to assist in wind turbine control which can be extended to develop relationships between the rotor effective wind speeds and the wind turbine loads. Using a less noisy wind turbine based rotor effective wind speed estimate, to correct the correlations between the corresponding measurements.

Acknowledgments

This work was carried out in the framework of the LAWINE project, funded by TKI Wind op Zee. The project partners ECN, the Netherlands, XEMC Darwind BV, the Netherlands and Avent Lidar Technology, France are hereby acknowledged for their contributions. I am thankful to G. Bergman and F. Savenije(ECN), R.Bos(TU Delft) and M. Boquet(Avent Lidar) for their support during meetings and discussions.

References

- [1] E. L. V. D. Hooft and T. G. V. Engelen, “Estimated Wind Speed Feed Forward Control for Wind Turbine Operation Optimisation,” *Wind Energy*, no. November, pp. 22–25, 2004.

- [2] W. Rietveld, *Wind speed feedforward control for a wind turbine using LIDAR*. Master thesis, Delft University of Technology, 2013.
- [3] E. Simley, L. Pao, and R. Frehlich, "Analysis of wind speed measurements using continuous wave lidar for wind turbine control," *49th AIAA Aerospace Sciences Meeting*, no. January, 2011.
- [4] E. Bossanyi, A. Kumar, and O. Hugues-Salas, "Wind turbine control applications of turbine-mounted LIDAR," *Proc. Science of Making Torque*, 2012.
- [5] D. Medici, S. Ivanell, J. Dahlberg, and P. H. Alfredsson, "The upstream flow of a wind turbine : blockage effect," *Wind Energy*, vol. 17, no. January, pp. 691–697, 2011.
- [6] G. Taylor, "The spectrum of turbulence," *Proceedings of the Royal Society of London, Series A, Mathematical and Physical Sciences*, vol. 164, no. Feb,18, 1938, pp. 476–490, 1938.
- [7] M. N. Soltani, T. Knudsen, M. Svenstrup, R. Wisniewski, P. Brath, R. Ortega, and K. Johnson, "Estimation of rotor effective wind speed: A comparison," *IEEE Transactions on Control Systems Technology*, vol. 21, no. 4, pp. 1155–1167, 2013.
- [8] F. Dunne, L. Y. Pao, D. Schlipf, and A. K. Scholbrock, "Importance of lidar measurement timing accuracy for wind turbine control," *Proceedings of the American Control Conference*, pp. 3716–3721, 2014.
- [9] D. Schlipf, "Lidar Assisted Control of Wind Turbines," tech. rep., Summer school in Remote sensing for Wind energy, 2012.
- [10] S. Raach, D. Schlipf, F. Haizmann, and P. W. Cheng, "Three Dimensional Dynamic Model Based Wind Field Reconstruction from Lidar Data," *Journal of Physics: Conference Series*, vol. 524, p. 012005, jun 2014.
- [11] R. Stull, *Practical Meteorology*. 2012.
- [12] Measnet, "MEASNET Procedure: Evaluation of Site Specific Wind Conditions, Version 1, November 2009.," Tech. Rep. November, Measnet Network of Wind Energy Institutes, 2009.
- [13] J. F. J. Manwell, J. G. J. McGowan, and A. L. a.L. Rogers, "Wind energy explained: theory, design and application. 2002," *John Wiley&Sons Ltd, UK*, pp. vii, 577 p., 2002.
- [14] IEC, "IEC 61400-12-1 Ed.1: Wind turbines - Part 12-1: Power performance measurements of electricity producing wind turbines," tech. rep., International Electrotechnical Commission, IEC, Geneva, Switzerland, 2005.
- [15] H.-J. Wagner, "Introduction to wind energy systems," *EPJ Web of Conferences*, vol. 54, pp. 1–15, 2013.
- [16] E. Simley and L. Y. Pao, "LIDAR Wind Speed Measurements of Evolving Wind Fields," *Proc. AIAA Aerospace*, no. July, 2012.
- [17] E. Simley, L. L. Y. Pao, P. Gebraad, and M. Churchfield, "Investigation of the Impact of the Upstream Induction Zone on LIDAR Measurement Accuracy for Wind Turbine Control Applications using Large-Eddy Simulation," *Journal of Physics: Conference Series*, vol. 524, p. 012003, jun 2014.
- [18] D. Medici, J. Dahlberg, and P. Alfredsson, "Measurements of the Flow Upstream a Rotating Wind Turbine Model," *Progress in Turbulence III*, 2009.
- [19] F. J. Savenije, "Analysis of the measurements on the AVENT five beam lidar prototype," Tech. Rep. August, 2014.
- [20] E. L. V. D. Hooft, P. Schaak, and T. G. V. Engelen, "Wind turbine control algorithms," no. December, 2003.
- [21] R. Bos, A. Giyanani, and W. Bierbooms, "Assessing the severity of wind gusts with lidar," *MDPI*, vol. Remote Sen, pp. 1–12, 2016.
- [22] A. Abdelsalam, "Méthodes de prédiction court terme de variabilité du vent par Lidar embarqué," tech. rep., AVENT Lidar Technology, Orsay, 2014.
- [23] D. Schlipf, F. Haizmann, N. Cosack, T. Siebers, P. W. Cheng, and N. Zealand, "Detection of Wind Evolution and Lidar Trajectory Optimization for Lidar Assisted Wind Turbine Control," 2014.
- [24] L. Ljung, *System Identification: Theory for the User*, vol. 25. New Jersey: PTR Prentice-Hall Inc., 1987.
- [25] A. K. Tangirala, *Principles of System Identification: Theory and Practice*. CRC Press, 2015.
- [26] J. Hong, M. Toloui, L. P. Chamorro, M. Guala, K. Howard, S. Riley, J. Tucker, and F. Sotiropoulos, "Natural snowfall reveals large-scale flow structures in the wake of a 2.5-MW wind turbine.," *Nature communications*, vol. 5, no. May, p. 4216, 2014.
- [27] W. Johnson, *Helicopter theory*. New York: Dover Publications Inc., 1st ed., 1980.
- [28] E. Bossanyi, "Un-freezing the turbulence: improved wind field modelling for investigating Lidar-assisted wind turbine control," *Proceedings of EWEA 2012*, 2012.
- [29] D. Schlipf, D. Trabucchi, O. Bischoff, and M. Hofsäb, "Testing of frozen turbulence hypothesis for wind turbine applications with a scanning lidar system," in *15th International Symposium for the Advancement of Boundary Layer Remote Sensing (ISARS)*, no. 3, 2010.
- [30] C. W. Higgins, M. Froidevaux, V. Simeonov, N. Vercauteren, C. Barry, and M. B. Parlange, "The Effect of Scale on the Applicability of Taylor's Frozen Turbulence Hypothesis in the Atmospheric Boundary Layer," *Boundary-Layer Meteorology*, vol. 143, pp. 379–391, 2012.